ISSN 0016-7932, Geomagnetism and Aeronomy, 2018, Vol. 58, No. 3, pp. 407–419. © Pleiades Publishing, Ltd., 2018.
Original Russian Text © A.T. Karpachev, 2018, published in Geomagnetizm i Aeronomiya, 2018, Vol. 58, No. 3.

Diurnal and Longitudinal Variations of the Structure of an Equatorial Anomaly During Equinoxes According to Intercosmos-19 Satellite Data

A. T. Karpachev*

Pushkov Institute of Terrestrial Magnetism, Ionosphere, and Radio Wave Propagation, Russian Academy of Sciences (IZMIRAN), Troitsk, Moscow, 108840 Russia

**e-mail: karp@izmiran.ru*

Received June 22, 2017; in final form, July 7, 2017

Abstract—Longitudinal and local time variations in the structure of the equatorial anomaly under high solar activity in the equinox are considered according to the Intercosmos-19 topside sounding data. It is shown that the anomaly begins to form at 0800 LT, when the southern crest is formed. The development of the equatorial anomaly is associated with well-known variations in the equatorial ionosphere: a change in the direction of the electric field from the west to the east, which causes vertical plasma drift W (directed upward) and the fountain effect. At 1000 LT, both anomaly crests appear, but they become completely symmetrical only by 1400 LT. The average position of the crests increases from $I = 20°$ at 1000 LT to $I = 28°$ at 1400 LT. The position of the crests is quite strong, sometimes up to 15°, varies with longitude. The *foF*2 value above the equator and the equatorial anomaly intensity (EAI) at 1200–1400 LT vary with the longitude according to changes in the vertical plasma drift velocity W. At this time, four harmonics are observed in the longitudinal variations of W, *foF*2, and EAI. The equatorial anomaly intensity increases to the maximum 1.5–2 h after the evening burst in the vertical plasma drift velocity. Longitudinal variations of *foF*2 for 2000–2200 LT are also associated with corresponding variations in the vertical plasma drift velocity. The equatorial anomaly intensity decreases after the maximum at 2000 LT and the crests decrease in size and shift towards the equator, but the anomaly is well developed at midnight. On the contrary, after midnight, *foF*2 maxima in the region of the anomaly crests are farther from the equator, but this is obviously associated with the action of the neutral wind. At 0200 LT, in contrast to the morning hours, only the northern crest of the anomaly is clearly pronounced. Thus, in the case of high solar activity during the equinoxes, a well-defined equatorial anomaly is observed from 1000 to 2400 LT. It reaches the maximum at 2000 LT.

DOI: 10.1134/S0016793218030076

1. INTRODUCTION

Interkosmos-19 (IK-19) is currently the unique satellite that has recorded the global distribution of electron density, including variations of *foF*2 and *hmF*2 at high solar activity. In this paper, the structure of the equatorial anomaly (EA) in *foF*2 is studied according to the IK-19 topside sounding data averaged for both equinoxes. There is nothing to compare with the comprehensive pattern (for all longitudes and hours of local time) of changes in the EA structure, which was obtained for the first time. However, a large number of results in some way related to the subject matter of this paper were obtained based on ground and satellite data. Therefore, the results of these studies were fully used in the paper for comparison and analysis. This primarily refers to the ground station data obtained in the American, Asian, and partly African longitudinal sectors (Rao, 1963; Rajaram, 1977; Walker, 1981; Sastri, 1990; Rao and Malthotra, 1964; Lyon and Thomas, 1963; Rastogi et al., 1972). Several studies were carried out with topside sounding data on the Alouette and ISIS satellites, which were also recorded only in the Asian and American longitudinal sectors (Sharma and Hewens, 1976; Eccles and King, 1969; Lockwood and Nelms, 1964; King et al., 1967; Rush et al., 1969). A large amount of total electron content (TEC) data has recently been received by GPS receivers that are land-bound and do not directly correlate with *foF*2 variations. Nevertheless, it is possible to note several interesting results obtained for the TEC at both high and low solar activity (Dabas et al., 2006; Zhao et al., 2009; Yizengaw et al., 2009). Several satellites conducted in situ measurements of the electron density at fixed altitudes and provided a global overview of the equatorial ionosphere. The data from the satellites that carried out *Ne* measurements at heights as close as possible to the height of the *F*2 layer can also be used for comparison. These satellites include Ariel (Hopkins, 1972) and especially CHAMP (Lui et al., 2007; Lei et al., 2010), the orbit of which was

almost at the heights of the maximum of the *F*2 layer of 350–450 km. Finally, a huge amount of data was obtained from radio occultation observations, especially in the FORMOSAT-3/COSMIC experiment. These data are global, but they mainly cover a period with low solar activity. Nevertheless, they are of great interest, since they reveal differences in the structure of the EA at different solar activity (Ram et al., 2009; Tsai et al., 2009; Yue et al., 2015).

2. OBSERVATIONAL DATA

The IK-19 satellite operated from March 1979 to February 1982. This period was characterized by high solar activity with an average value of $F10.7 \sim 200$. The satellite was in an elliptical orbit with altitudes of 500–1000 km and an inclination of 74°. An onboard recording device made it possible to record digital ionograms at any longitude within the orbital inclination. The Jackson method (Jackson, 1969) was applied to ionograms to calculate the $N(h)$ profiles of the topside ionosphere, which gave values of *foF*2 and *hmF*2. These values were used to construct the distribution of the parameters of the maximum of the *F*2 layer in the region of the equatorial anomaly within the ±70° geomagnetic inclination. Equinoxes occur in March–April and September–October, i.e., for eight months in the two years of satellite operation. In total, 30000 pairs of *foF*2 and *hmF*2 values for quiet conditions $Kp \leq 3$ were obtained for this period. This was insufficient for a separate presentation of spring and autumn equinoxes. Therefore, they are considered together in the paper. However, this data is sufficient to build 12 so-called LT-maps every 2 h of local time, i.e., one map has ~2000 values of *foF*2 or *hmF*2. The maps were constructed with the routine Surfer software by the inverse distance method. The data for each map uniformly covered all longitudes; thus, a fairly smooth distribution of *foF*2 and *hmF*2 was obtained, which indirectly confirms the adequacy of the obtained data. In this paper, we consider only the *foF*2 variations.

3. EQUATORIAL ANOMALY DEVELOPMENT

Let us consider the dynamics of the equatorial anomaly development depending on local time at all longitudes. Figure 1 shows the distributions of *foF*2 in the EA region for 0800, 1000, 1200, and 1400 LT. Figure 2 shows the latitudinal cross-sections of *foF*2 for the characteristic longitudinal sectors of 90°, 210°, and 270°. The longitudinal sectors 90° and 270° differ most strongly in the deviation of the geographical equator with respect to the geomagnetic one, and the equators almost coincide in the longitudinal sector of 210°. In the morning, the EA is most strongly developed in the longitudinal sector 90°; conversely, it is the most underdeveloped in the longitudinal sector 210°. The EA begins to show up as a structure at ~0800 LT. First, the southern crest of the anomaly appears, even though this equinox and the conditions for the formation of crests in the Northern and Southern Hemispheres seem to be the same. The southern crest is clearly seen at longitudes 30°–300°. A weak northern crest appears only in the longitudinal sector of 300°. Note that, in the longitudinal sectors of 210° and 270° in Fig. 2, it is also possible to detect small maxima of *foF*2 in the Southern Hemisphere, but they are too far from the equator to be associated with the action of the fountain effect, i.e., with the EA. At 1000 LT, the electron density in the entire ionosphere increases sharply, especially in the longitudinal sector of 270°. The asymmetry of the northern and southern crests as a whole decreases but still remains significant in the longitudinal sector of 210°, where the original difference between the Northern and Southern Hemispheres was especially large. Although the northern crest is smaller than the southern crest, it is fixed quite clearly at all longitudes. In the literature, there has long been debate over the longitudinal sector in which the EA first develops, both from ground-based (Rajaram, 1977; Rao and Malthotra, 1964; Lyon and Thomas, 1963) and satellite (Hopkins, 1972; Sharma and Hewens, 1976; Eccles and King, 1969; Lockwood and Nelms, 1964) data. The opinions of different authors differed, but most agreed that the EA develops earlier in the Asian sector than in the American sector. For example, Hopkins (1972) used Ariel 4 data to show that, at high solar activity, the EA at longitudes of 90°–120° exists continuously already at 1000 LT; at longitudes of 180°–270°, it forms only after 1200 LT. Sharma and Hewens (1976) clarified this thesis, stating that the EA appears in the American longitudinal sector at 0800 LT under low solar activity and 4 h later at high activity. Let us try to answer this question according to the IK-19 data presented in Figs. 1 and 2. Figure 1 shows that a weak *foF*2 maximum is seen only in the Northern Hemisphere in the longitudinal sector of 300° at 0800 LT at latitudes inherent in the EA crest. Even at 1000 LT, the northern crest is much smaller than the southern crest at all longitudes. However, the longitudinal difference is insignificant, and it is therefore impossible to state clearly that the EA appears at some longitudes earlier than at the others. It is only possible to repeat that the EA is more strongly developed in the longitudinal sector of 90° than at other longitudes.

A specific EA structure inherent only to the equinox forms at 1000–1200 LT, since the equatorial trough is shallow; the crests are poorly developed but occupy a wider latitudinal range than in winter or summer. By 1200 LT, the electron density in the anomaly crests increases rather strongly. Thus, its development continues. The anomaly crests begin to match in magnitude with the southern crest forming at all longitudes. By 1400 LT, the electron density in the equatorial ionosphere is even greater, especially in the longitudinal sector of 90°. The EA becomes even more

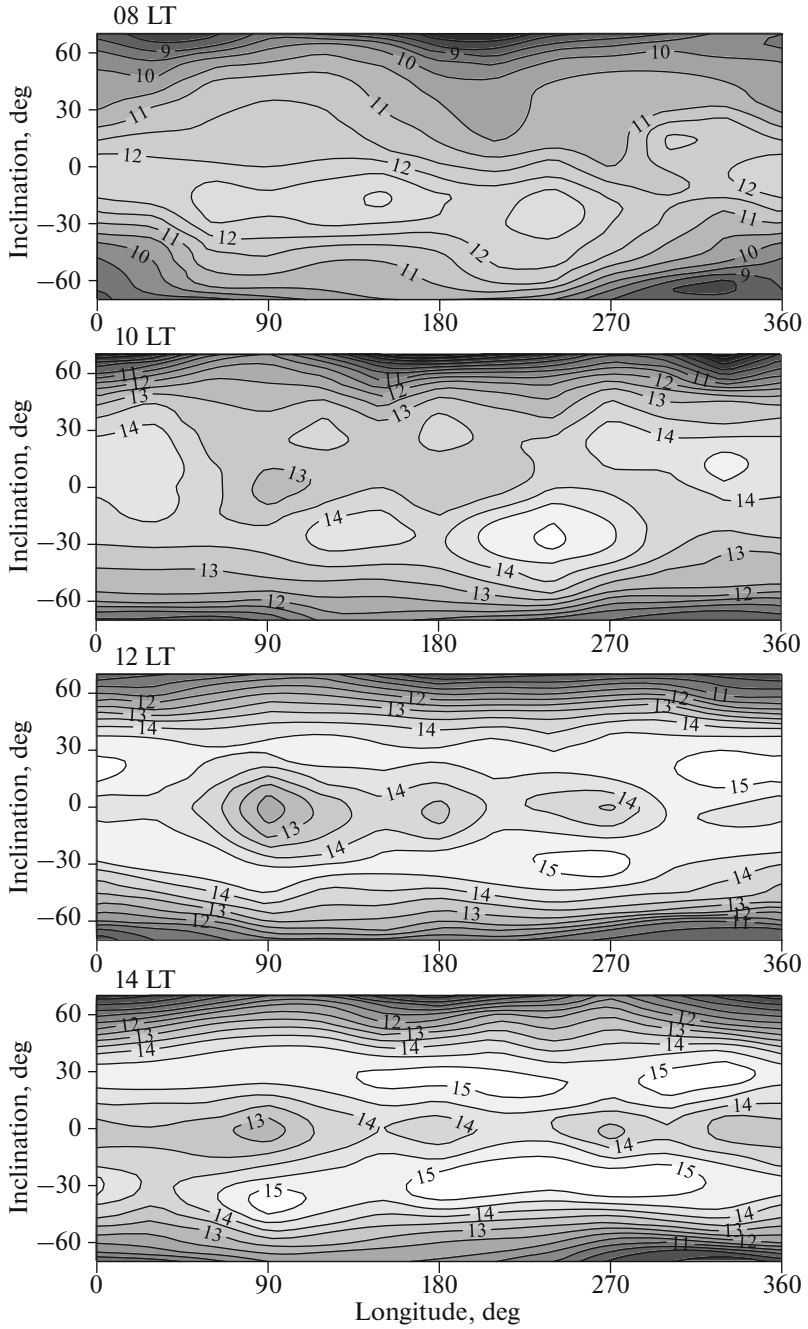

Fig. 1. *foF*2 distributions in the equinox during EA development for 0800, 1000, 1200, and 1400 LT.

developed with well-marked crests. Figure 2a shows the difference between the latitudinal variations of *foF*2 at different longitudes, which is observed at 1400 LT. The EA is most strongly developed in the longitudinal sector of 90°. Consequently, the anomaly crests are farthest from the equator, and the electron density in the trough above the equator is minimal. Conversely, the EA is least developed in the longitudinal sector of 210°. The southern crest at all longitudes is slightly larger than the northern crest. This is inconsistent with the conclusions (Rajaram, 1977; Rao and Malthotra, 1964), in which the EA was observed in March 1958 and in which it was claimed that the northern crest is larger all day in the Asian sector and that the southern one is larger in the American sector. Ram et al. (2009) considered EA development in the equinox according to the COSMIC experiment data for 2007. These data refer to very low solar activity. It is even more interesting that they show a very similar behavior of the EA during its development. Figure 6 from this work shows

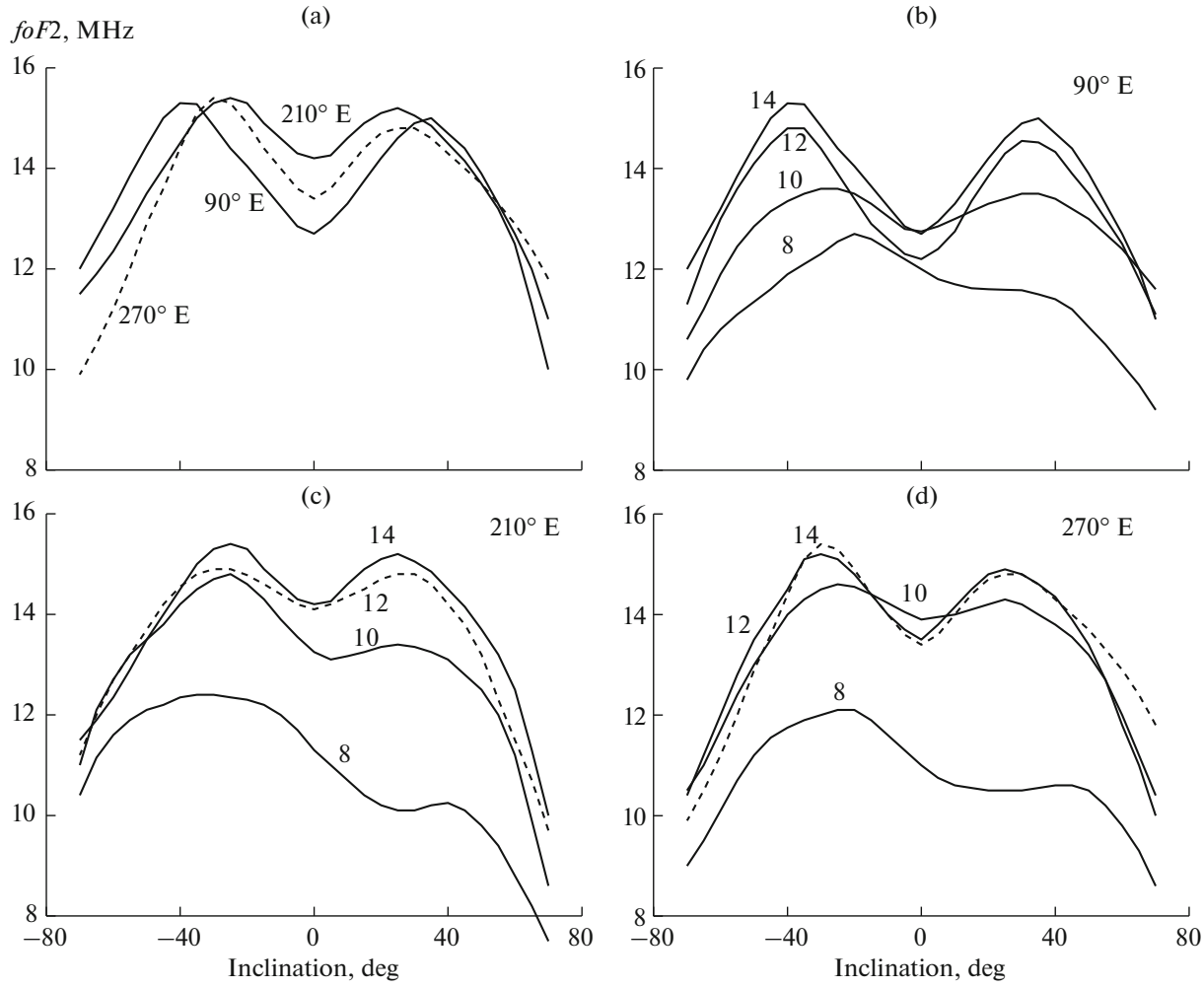

Fig. 2. Latitudinal profiles of *foF*2 in different longitudinal sectors for 0800, 1000, 1200, and 1400 LT (b, c and d). Figure 2a gives latitudinal variations of *foF*2 at longitudes of 90°, 210°, and 270° for 1400 LT for comparison.

that the EA is asymmetrical from 0700 to 1100 LT, since the southern crest predominates. This is particularly evident in the central Pacific region, i.e., at longitudes of 180°–270°. Ram et al. (2009) associated this EA behavior with the fact that the magnetic declination at these longitudes is positive (to the east). Thus, a strong western neutral wind in the morning hours (Wu et al., 1994) carries plasma along geomagnetic field lines to the Southern Hemisphere. After 1100 LT, under the impact of the vertical drift, the fountain effect dominates over the neutral wind, and the EA becomes symmetrical.

Figure 3 below shows longitudinal variations of the position of the northern and southern crests of the EA for 0800–1400 LT. In fact, their dynamics during EA development was discussed above. First, the southern crest of the anomaly appears; the northern crest at 0800 LT forms only at longitudes of 300°–330°. However, the northern crest is already observed at 1000 LT at all longitudes, and the southern crest forms at all longitudes only by 1200 LT. The developed EA with well-formed crests is formed only by noon. As the EA develops, the crests move farther from the equator. The most distant crests are separated from the equator in the longitudinal sector of 90°, where the most developed EA is observed. The total width of the EA crests at 1400 LT in terms of the magnetic declination reaches 70°*I* in the longitudinal sector of 90° and 50°*I* in the longitudinal sector of 270°. This is inconsistent with the data of the Alouette satellite for the American sector, according to which the EA width was 70°*I* at high solar activity (58°*I* at low) (Sharma and Hewens, 1976).

The solid curve in the middle panel of Fig. 3 shows the EAI longitudinal variations as the ratio of *foF*2 in the crests to *foF*2 in the equatorial trough, i.e., EAI = $foF2_C/foF2_E$. The *foF*2 values in the northern and southern anomaly crests were averaged. EAI variations were obtained by averaging the data for 1200–1400 LT; they are presented in Fig. 3 with longitudinal resolution of 30°. For comparison, longitudinal variations of

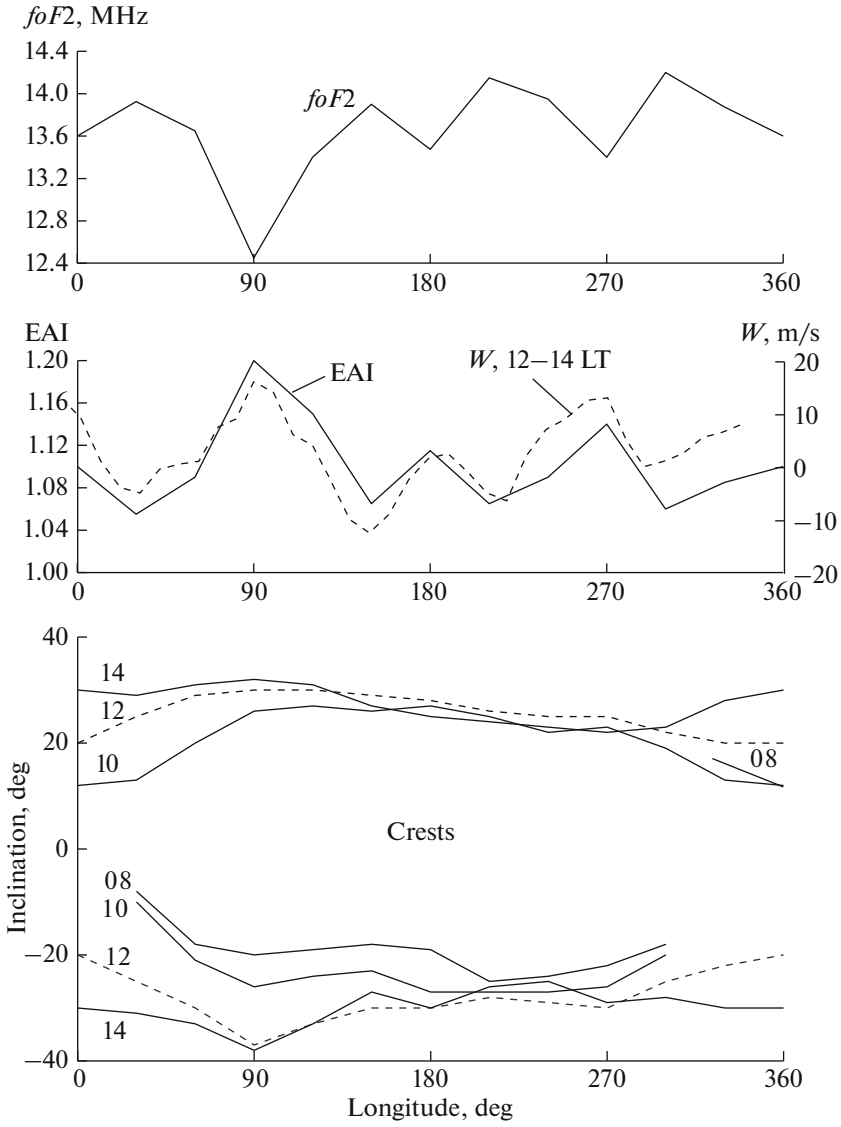

Fig. 3. Top: longitudinal variations of *foF*2 above the equator for 1200–1400 LT. Middle: variations in the EAI (solid curve) and vertical plasma drift velocity (dashed curve) from the ROCSAT data also for 1200–1400 LT (Oh et al., 2008). Bottom: changes in the position of the anomaly crests for 0800, 1000, 1200, and 1400 LT.

the velocity of the vertical plasma drift W above the equator are shown by the dashed curve. They were obtained from the ROCSAT-1 satellite data for 1200–1400 LT for equinox periods in 1999–2002, i.e., also for high solar activity (Oh et al., 2008). For clarity, variations in the drift velocity are shifted by 15° to the west. With such a representation, it can be clearly seen that variations in the EAI and the drift velocity above the equator are very close, especially if the variations of both quantities are obtained by averaging of the data over a relatively wide interval of local time and presented with different longitudinal resolutions. The *foF*2 variations over the equator are shown in the top panel of Fig. 3. They are also averaged for 1200–1400 LT. It is clear that the EAI is determined mainly by *foF*2 variations over the equator, which, in turn, are determined by variations in the vertical plasma drift velocity. This is a well-known fact; only the high consistency of all the of the studied quantities is surprising. In the longitudinal variations of all the parameters, the fourth harmonic is clearly dominant, which is reflected in the recently intensified 4-wave concept (for example, (Ram et al., 2009)). It assumes the influence of the lower atmosphere on the ionosphere of the E region, and, consequently, on the magnitude of the vertical drift (for example, (Pancheva and Mukhtarov, 2012) and references therein).

4. DAY CONDITIONS

Let us consider the EA behavior further, throughout the day. Figure 4 shows the distribution of *foF*2 for

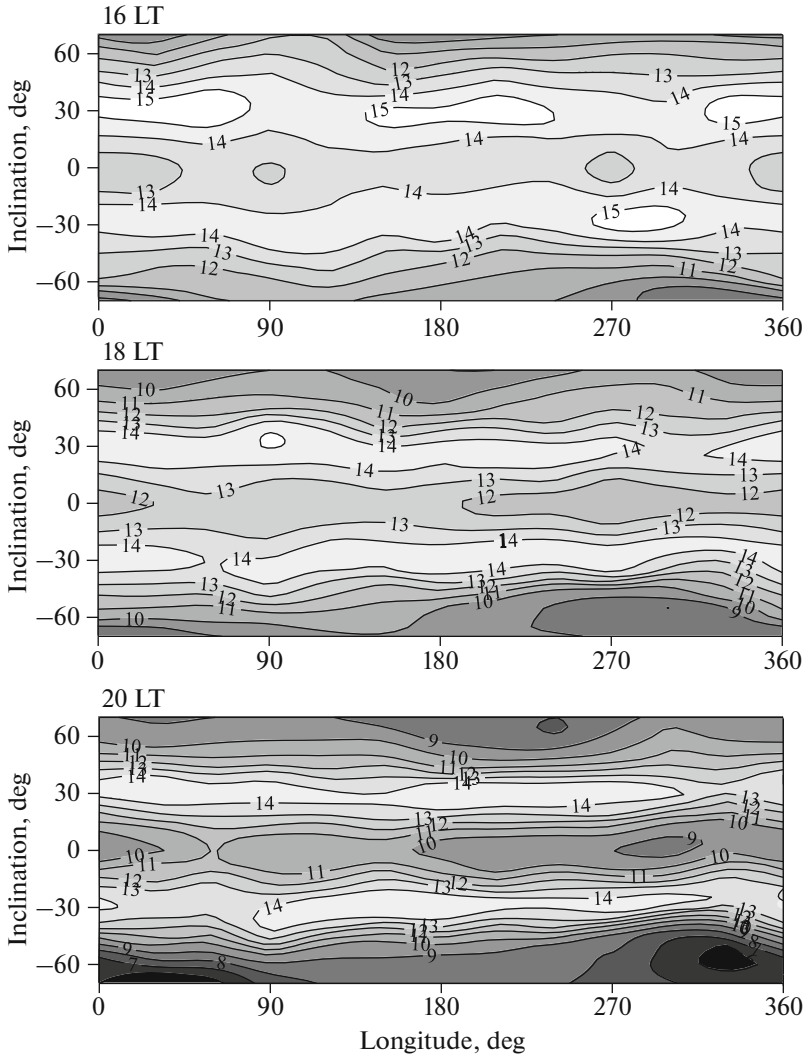

Fig. 4. *foF*2 distributions in the equinox period for day/evening hours (1600, 1800, and 2000 LT).

1600, 1800, and 2000 LT, and Fig. 5 presents the latitudinal profiles of *foF*2 for these instants in the longitudinal sector of 90°. The EA dynamics in afternoon/evening hours can be clearly traced in both figures. The electron density at the peaks of the crests remains constant, ~15 MHz. At the same time, the electron density at low/middle latitudes decreases toward the evening with a decrease in the illumination of the ionosphere. The electron density over the equator also decreases, since the vertical drift velocity increases from 1600 LT, which is well known and will be demonstrated below. As a result, the crest width decreases, and the EAI increases and reaches maximum values by 2000 LT. In other words, the EA in the evening is most pronounced. In the longitudinal variations of *foF*2 over the equator, four harmonics can be traced for the entire time. However, the 4-wave concept requires a more in-depth analysis and is not considered here.

The entire EA structure changes quite a lot with longitude. Figure 5 also shows the latitudinal *foF*2 variations for 2000 LT in the longitudinal sector of 270° for comparison with the longitudinal sector of 90°. During the development period, the EA was the most developed in the longitudinal sector of 90°. However, the EA structure changes over time and becomes the most developed in the longitudinal sector of 270°–300°. It happens again due to a decrease in the electron density above the equator, since the crest size remains almost the same. In addition, the EA becomes strongly asymmetrical at longitudes of 270°–300°, because *foF*2 in the Southern Hemisphere sharply decreases on the outer slope of the southern crest of the anomaly. The reasons for this electron density behavior in the Southern Hemisphere also require separate analysis. The most stable EA characteristic during the day is the position of EA crests. Neither longitudinal variations nor the average position vary strongly.

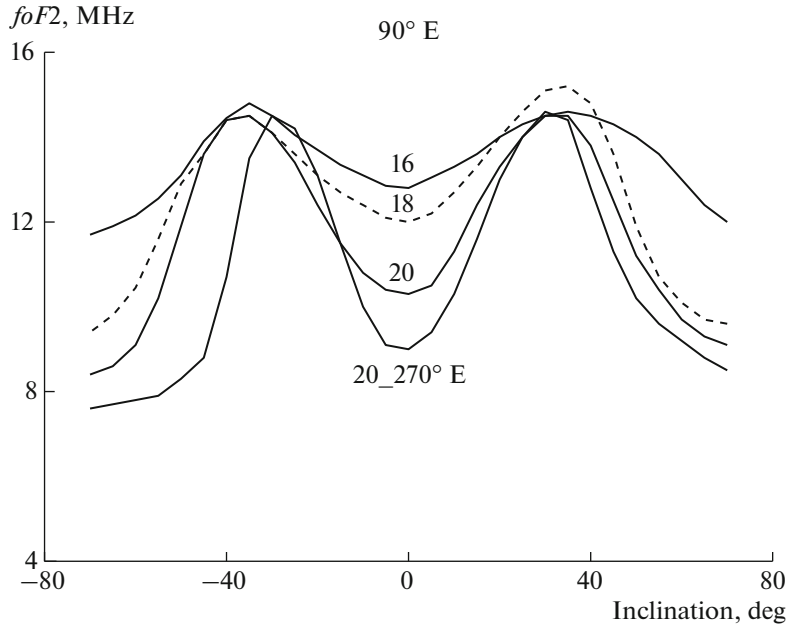

Fig. 5. Latitudinal profiles of *foF*2 in the longitudinal sector of 90° for 1600, 1800, and 2000 LT and in the longitudinal sector of 270° for 2000 LT.

5. EQUATORIAL ANOMALY DECAY

Finally, let us consider EA decay. Figure 6 shows the *foF*2 distributions for 2200, 2400, 0200, and 0400 LT, and Fig. 7 shows the latitudinal variations of *foF*2 for these local times for different longitudinal sectors. Analysis of both figures shows that the electron density at midlatitudes decreases even more over time by 2200 LT, not only in the Southern but also in the Northern Hemisphere. At the equator, *foF*2 slightly increases at 2000–2200 LT, so the EA after the maximum at 2000 LT begins to decrease. This process continues even further, but the EA is still very well developed at midnight, which contrasts sharply with the EA behavior at low activity, when it almost disappears by 1800–1900 LT (Ram et al., 2009). After midnight, the southern crest decays much faster than the northern one, i.e., the EA asymmetry is reversed in comparison with that observed in EA development. However, even at 0200 LT at longitudes of 240°–340°, there is a clearly expressed EA, so the EA exists the longest in the American longitudinal sector. The electron density in the EA region decreases sharply according to the daily cycle and due to the weakening of the fountain effect (Fejer et al., 2008). By 0400 LT, the EA decays completely. There are only individual maxima of electron density at low latitudes, i.e., formally, crests move away from the equator. Figure 8 shows variations in the position of the EA crests during its decay. At 2000 LT, as one would expect, the crests are on average located farthest from the equator. They undergo longitudinal variations, especially strong in the Southern Hemisphere, such that the crests farthest from the equator are in the longitudinal sectors of 90°–270°. After midnight, the EA begins to decay rapidly, so the crests move to the equator, which again reflects the typical EA behavior. However, at 0200–0400 LT, both in the Northern and Southern Hemispheres, the remnants of the crests are on average located farther from the equator than at midnight. To what extent these maxima are related to the normal EA crests remains unclear. Thus, their behavior in the Northern Hemisphere is determined by the usual longitudinal effect in the midnight midlatitude ionosphere (for example, the publication (Klimenko et al., 2016)). In the Southern Hemisphere, the *foF*2 maximum at longitudes of 240°–300° is undoubtedly a reflection of the Weddell Sea anomaly (WSA), which is most clearly manifested in nighttime summer conditions (for example, (Klimenko et al., 2015)). This maximum is purely formally shown in Fig. 8 as an EA crest. In both hemispheres, this indicates that the neutral wind has a greater effect than the electric field that creates the EA.

Variations in the EAI for evening hours are given in the top panel of Fig. 8. In order to eliminate random variations, they were obtained via averaging of the data for 2000–2200 LT. The dashed curve also shows the longitudinal variations of the vertical plasma drift velocity W above the equator from the ROCSAT satellite data. They were calculated (from Fig. 2 of Ren et al., 2011) for the periods of the autumn equinox of 1999–2004 for the time 1800 LT. The W values can be considered from this figure only approximately. The minimum is observed in them at longitude of 300°, which is noncharacteristic for the EAI. The data refer to 1800 LT. The nature of the changes in W for the

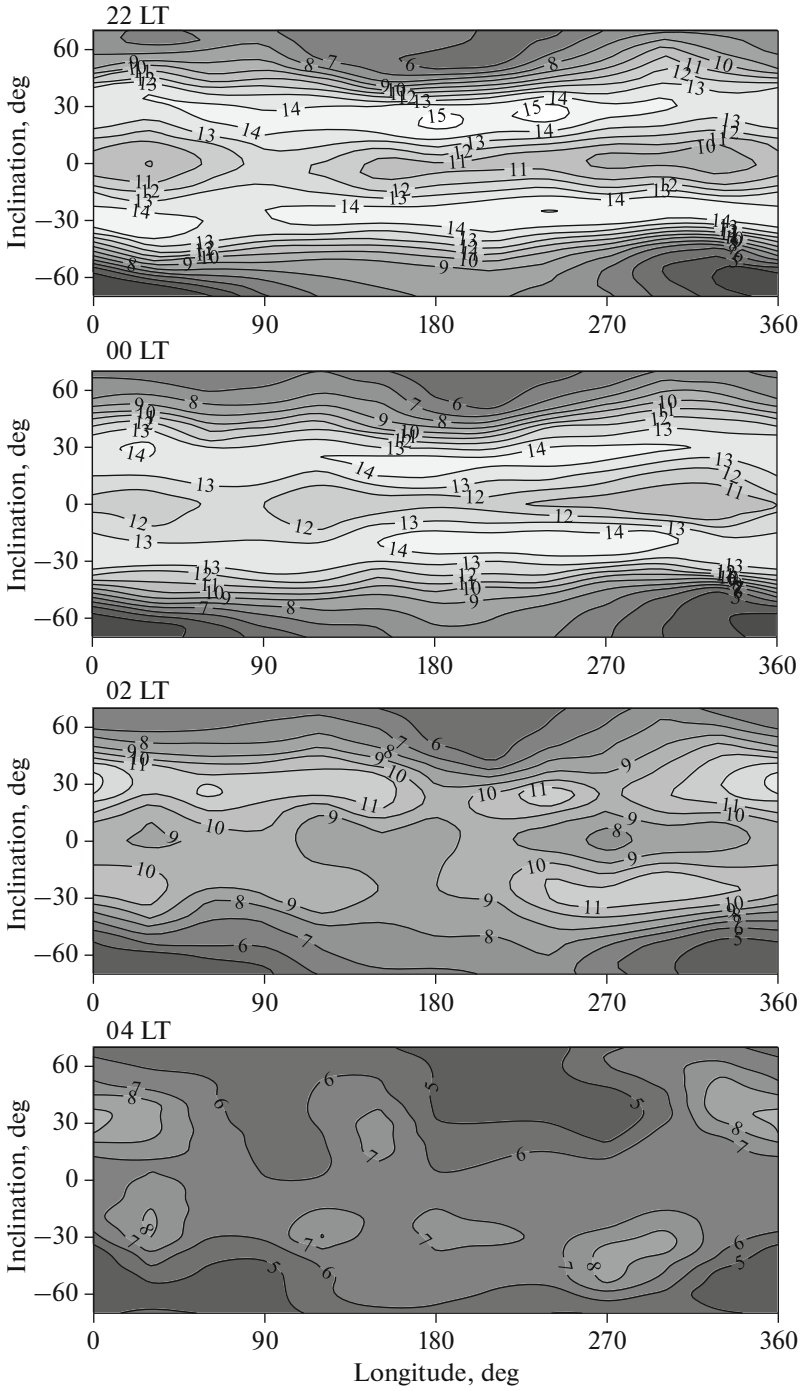

Fig. 6. *foF*2 distributions in the equinox during EA decay for 2200, 2400, 0200, and 0400 LT.

spring equinox is different. Therefore, these data should be treated with caution. Nevertheless, there is a surprising agreement between the EAI longitudinal variations and the vertical plasma drift velocity *W* in the evening hours. A very similar EA behavior in the evening was observed from *Ne* measurements on the Hinotori satellite (Su et al., 1996) during the equinox at high solar activity: the EA was most developed around 2000 LT, and the EAI varied with longitude from 1.15 in the Eastern Hemisphere to 2.0 in the Western. The absolute values of the EAI are somewhat smaller than in Fig. 8, since the Hinotori satellite conducted in situ measurements not at the maximum of the *F*2 layer but at heights of ~600 km.

Lastly, the middle panel of Fig. 8 shows the longitudinal variations of *foF*2 over the equator. They were

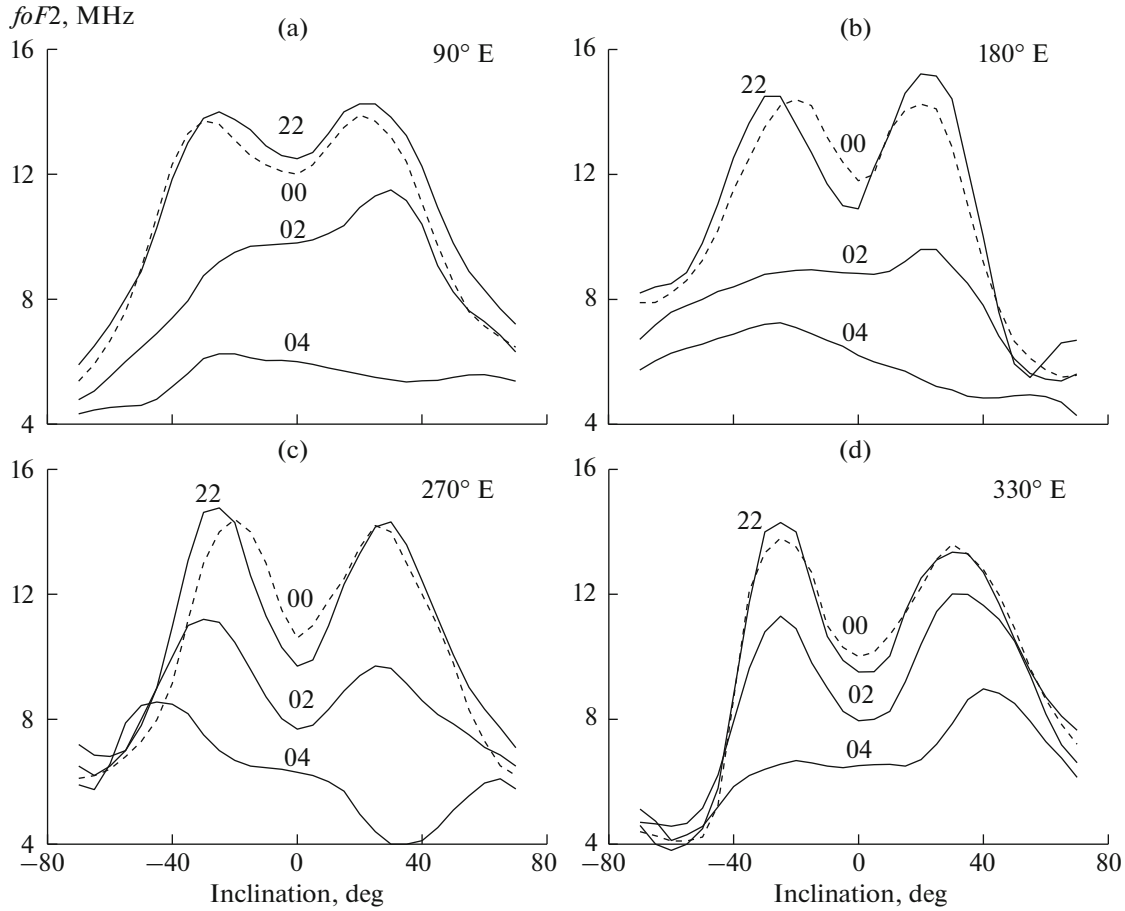

Fig. 7. Latitudinal variations of *foF*2 for 2200, 2400, 0200, and 0400 LT in the longitudinal sectors 90°, 180°, 270°, and 330°.

also obtained via averaging of the data for 2000–2200 LT. Since *foF*2 at the crest maxima varies only slightly, it is clear that the EAI longitudinal variations in the evening, as well as in the daytime, are determined mainly by the *foF*2 variations over the equator, which in turn are determined by vertical plasma drift variations.

Since the vertical drift velocity varies greatly with longitude, not only *foF*2 but the entire electron density profile will vary with longitude. Figure 9 shows $N(h)$ profiles for characteristic longitudinal sectors obtained on April 22–23, 1980, in quiet (Kp = 2–3) evening conditions (2118–2136 LT). The first profile was obtained on April 22 at 1653:30 UT at a longitude of 65° and a latitude of −0.7°*I*. The second profile was obtained on April 23 at 0116:58 UT at a longitude of 300° and a latitude of −2.5*I*. Figure 9 shows that the electron density at all altitudes of the topside ionosphere is much larger and *hmF*2 is much smaller at a longitude of 65° than at longitude of 300°, as one could assume from the mechanism of the fountain effect. However, an additional equatorial layer *F*3 forms in the evening almost 40% of the time (Karpachev et al., 2013). This case is represented on the plot by the third profile obtained on April 23 at 0256:10 UT at a longitude of 280° and a latitude of −0.6°*I*. When the *F*3 layer forms, the situation changes dramatically: the height of the *F*2 layer maximum drops very sharply, and a small local maximum of the electron density, which represents the *F*3 layer, forms in the topside ionosphere at a height of ~650 km.

6. EQUATORIAL ANOMALY DIURNAL VARIATIONS

Let us consider the diurnal variation of the EA characteristics. Figure 10 (bottom) shows diurnal variations of the EAI. They were obtained via averaging of the data separately for longitudes of 60°–120° and 240°–300°. The vertical plasma drift variations determined for the equinox according to the ROCSAT data in (Fejer et al., 2008) are also given there. The EA starts to form at 0800 LT, but, as shown above and in Fig. 10 (middle), there is only one, southern, crest at this time. Therefore, the EAI value was set to 1. At 1000 LT, both EA crests appear, and the EAI begins to increase. It is clear that this occurs after a change in the direction of the vertical plasma drift velocity. The EAI value is relatively slowly increasing by 1800 LT,

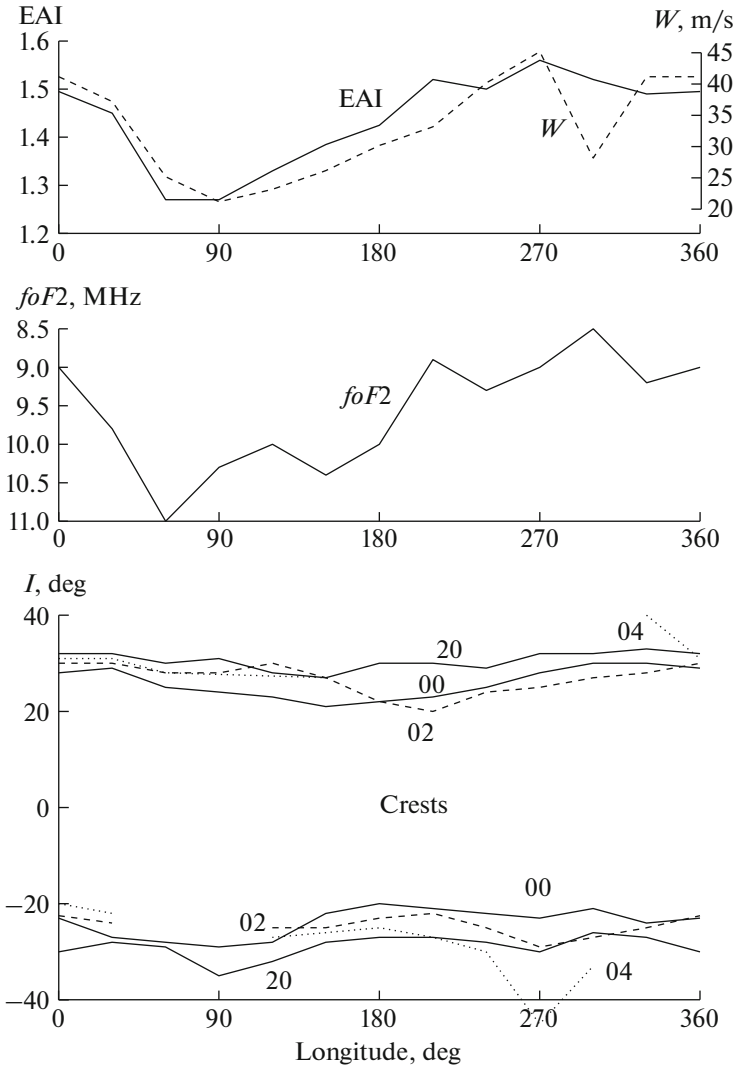

Fig. 8. Middle: longitudinal variations of *foF*2 above the equator for 2000–2200 LT. Top: EAI variations (solid curve) and the vertical plasma drift velocity (dashed curve) from the ROCSAT data also for 2000–2200 LT (Ren et al., 2011). Bottom: changes in the position of the anomaly crests for 2000 LT (solid curve), 2400 LT (solid), 0200 LT (dashed), and 0400 LT (dashed).

monotonically, at the longitudes of the Western Hemisphere; at the longitudes of the Eastern Hemisphere, it has a local maximum at 1200–1400 LT, which is clearly associated (with a fully understandable delay) with a local maximum of the plasma drift velocity at 1000–1100 LT. This maximum was even more clearly recorded earlier according to the data of the ISS-b satellite for August–December 1979 (Matuura, 1981). This maximum manifested itself particularly strongly in the sector of 90°–120°. The EAI noon maximum is associated with the noon decrease in *foF*2, which is observed in the form of the so-called bite-out specifically at Indian longitudes (Rao, 1963). The EAI quickly reaches a maximum of EAI ~1.5 around 2000 LT, i.e., with a delay of 1.5–2 h after the evening burst in the vertical plasma drift velocity. The IK-19 data does not make it possible to determine this delay more accurately. After that, the EAI value drops sharply to midnight and further to 0200 LT.

Variations in the location of the EA crests were obtained via averaging of the data for all longitudes. Figure 10 shows that the crest maxima are formed by ~20°*I*, and then they are shifted from the equator to ~28.5°*I* at 1400 LT (the total width of the EA is 57°*I*). At the same time, the southern crest is ahead of the northern crest. The EA crests are farthest from the equator at 2000 LT (the overall width of the EA reaches 59°*I*); they then shift back to the equator until midnight. Lui et al. (2007), according to the CHAMP data at an altitude of 400 km, give somewhat different widths of the crests: ~58° at noon and ~70° in the evening. (At low solar activity at noon, the width is 45° and decreases to 30° in the evening). Unfortunately, the paper does not report how these values were obtained.

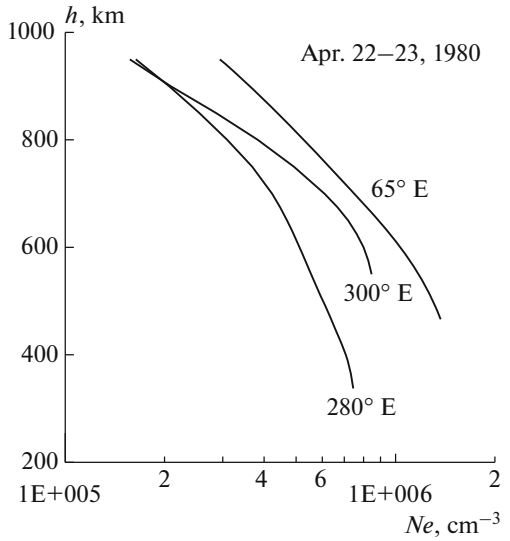

Fig. 9. Profiles of electron density obtained on Apr. 22–23, 1980, in quiet evening conditions at different longitudes above the equator.

Therefore, it can be assumed that the discrepancies can be associated with strong longitudinal variations in the position of the crests.

Both EA crests remain at 0200 LT, though not at all longitudes, and the EAI is still quite high. After 0200 LT, the crests in Fig. 10, on the contrary, are displaced from the equator. However, as shown above, the electron density maxima at the crest latitudes at this time are related to the action of the neutral wind rather than to the electric field forming the EA. Therefore, the EAI value at 0400 LT was also set to 1. Figure 10 (top) shows the diurnal variations of *foF*2 above the equator and at the crest maxima for the longitudinal sector of 90° as an example. The lowest *foF*2 values are observed at 0400–0600 LT. After sunrise *foF*2 sharply increases to 1200 MHz by 0800 LT. At this time, the crests begin to form with an electron density somewhat higher than above the equator. By 1400 LT, *foF*2 in the crests increases to ~15 MHz, and then decreases slightly by midnight. In this case, the *foF*2 value in both crests shows

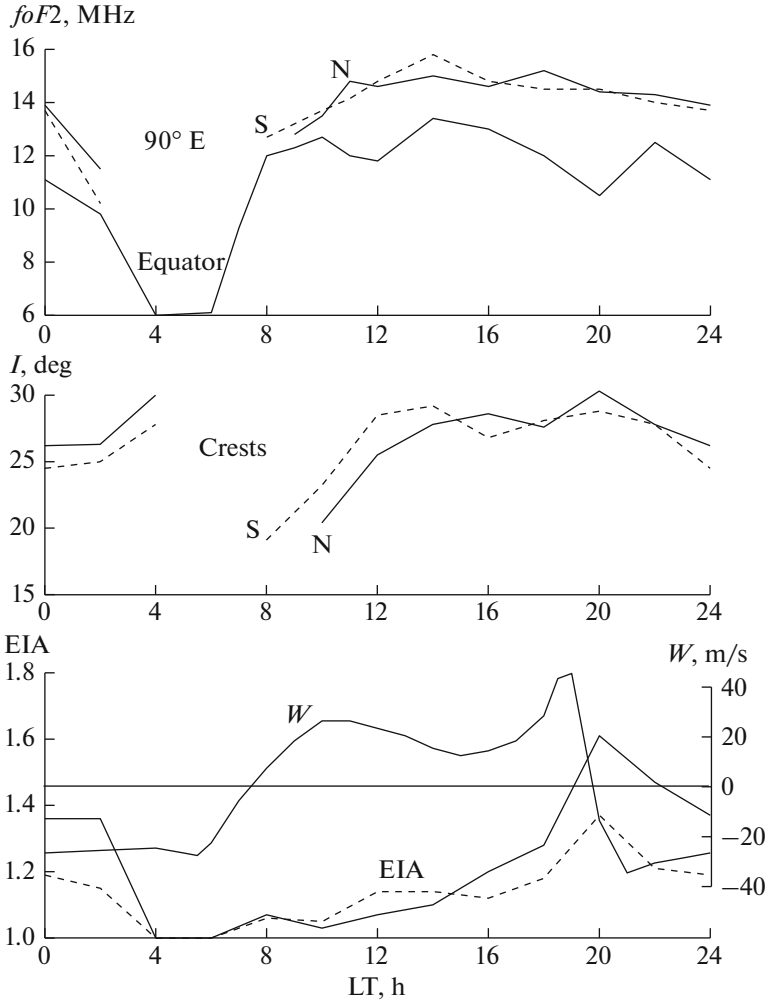

Fig. 10. Top: diurnal variations of *foF*2 at the longitude of 90° above the equator and also at the maximum of the northern (N) and southern (S) crests. Middle: variations in the location of EA crests in the Northern and Southern Hemispheres. Bottom: variations in the vertical plasma drift velocity (Fejer et al., 2008) and EAIs at longitudes of 60°–120° (dashed curve) and at longitudes 240°–300° (solid curve).

significant longitudinal variations, but both crests are almost symmetrical at a fixed longitude. This is a distinctive feature of the equinox compared to the solstices. After midnight, *foF*2 drops sharply by 0400 LT in the entire ionosphere. Note also that *foF*2 above the equator in the longitudinal sector of 90° reflects both EAI peaks at 1200 and 2000 LT. The electron density in the EA crests does not change noticeably at this time.

The movement of crests away from the equator after ~0200 LT is consistent with ground-based observations made in the Asian sector in (Walker et al., 1994). The authors claimed that there is a resurgence of the EA crests around 0300 LT at high solar activity in any season. An even stronger assertion was made in a work (Yizengaw et al., 2009) in which, according to TEC TOPEX at 80° W on April 27, 2003, an EA maximum was observed at 2000 LT, a minimum was observed at 2318 LT, and a well-developed EA was then again observed up to up 0400 LT. According to IK-19, a similar EA behavior was first discovered, but an intermediate result was obtained after more careful data processing: the crests at 0200 LT do move away from the equator, but the EAI continuously decreases after 2000 LT. Thus, the effect reported by Yizengaw et al. (2009) is apparently not always observed.

7. DISCUSSION AND CONCLUSIONS

Let us summarize the study of the EA dynamics with local time during the equinox at high solar activity and compare with the results for low solar activity. The EA begins to form at 0800 LT and at low solar activity. First, the southern crest of the anomaly appears; up to ~1400 LT, it develops faster than the northern crest, i.e., the EA anomaly is asymmetrical for all of this time. The EA development is clearly associated with a change in the direction of the electric field to the east, after which the vertical plasma drift W is directed upward and the fountain effect comes into action. The crests become completely symmetrical only by 1400 LT. They move away from the equator from 20°I at 1000 LT to 28°I at 1400 LT. These are the values obtained via averaging of the data for all longitudes. In fact, the crest position significantly changes with longitude. The *foF*2 value above the equator and the EAI at 1200–1400 LT vary with longitude according to changes in the vertical plasma drift velocity (Oh et al., 2008). The averaged EAI then monotonically increases to 1800 LT. However, at some longitudes (especially 90°–120°), there is a local EAI maximum around noon that is associated with the local maximum in the vertical plasma drift velocity. The EA structure is the stablest at noon, from about 1400 LT to 1800 LT. The EAI increases dramatically to EAI = 1.5–2 h after the evening burst in vertical plasma drift velocity. At the same time, *foF*2 drops over the equator, and the crests move away from the equator a little, as one would expect. Thus, the EA development reaches its maximum at about 2000 LT, which is much later than at low solar activity (at 1600–1700 LT) (Ram et al., 2009). The longitudinal variations of *foF*2 for 2000–2200 LT, as well as at 1200–1400 LT, are clearly associated with variations in the vertical plasma drift velocity for this period (Ren et al., 2011). The EAI decreases after the maximum at 2000 LT, but the EA is very well developed even at midnight, in contrast to the low solar activity, in which it decays already by 1900–2000 LT (Ram et al., 2009). The EA exists the longest in the American longitudinal sector: up to 0200 LT at high solar activity and up to 2100–2400 LT at low solar activity (Sharma and Hewens, 1976). The *foF*2 values decrease with decreasing illumination of the ionosphere throughout the EA region, and the crests decrease in magnitude and move to the equator until midnight. After that, the *foF*2 maxima in the region of EA crests, on the contrary, are farther from the equator, but this is obviously associated not with the action of the electric field but with the neutral wind. At 0200 LT, only the northern crest of the anomaly is clearly pronounced; the weaker southern crest is not observed at all longitudes. At 0400 LT, only the remainders of the EA are observed. Thus, at high solar activity during the equinox, a pronounced EA is observed from about 1000 to 2400 LT.

ACKNOWLEDGMENTS

This work was supported by the Program of the Presidium of the Russian Academy of Sciences, project no. 7.

REFERENCES

Dabas, R.S., Singh, L., Garg, S.C., Das, R.M., Sharma, K., and Vohra, V.K., Growth and decay of a post-sunset equatorial anomaly at low latitudes: Control of ExB, neutral winds and daytime electrojet strength, *J. Atmos. Sol.-Terr. Phys.*, 2006, vol. 68, no. 14, pp. 1622–1632.

Eccles, D. and King, J.W., A review of topside sounder studies of the equatorial ionosphere, *Proc. IEEE*, 1969, vol. 57, no. 6, pp. 1012–1018.

Fejer, B.G., Jensen, J.W., and Su, S.-Y., Quiet time equatorial *F* region vertical plasma drift model derived from ROCSAT-1 observations, *J. Geophys. Res.*, 2008, vol. 113, A05304. doi 10.1029/2007JA012801

Hopkins, H.D., Longitudinal variation of the equatorial anomaly, *Planet. Space Sci.*, 1972, vol. 20, no. 12, pp. 2093–2098.

Jackson, J.E., The reduction of topside ionograms to electron-density profiles, *Proc. IEEE*, 1969, vol. 57, no. 6, pp. 960–976.

Karpachev, A.T., Klimenko, M.V., Klimenko, V.V., and Kuleshova, V.P., Statistical study of the *F*3-layer characteristics retrieved from Intercosmos-19 satellite data, *J. Atmos. Sol.-Terr. Phys.*, 2013, vol. 103, no. 10, pp. 121–128.

King, J.W., Olatunji, E.O., Eccles, D., and Newman, W.S., The integrated electron content in the equatorial iono-

sphere, *J. Atmos. Terr. Phys.*, 1967, vol. 29, no. 11, pp. 1391–1396.

Klimenko, M.V., Klimenko, V.V., Karpachev, A.T., Ratovsky, K.G., and Stepanov, A.E., Spatial features of Weddell Sea and Yakutsk anomalies in *foF*2 diurnal variations during high solar activity periods: Interkosmos-19 satellite and ground-based ionosonde observations, IRI reproduction and GSM TIP model simulation, *Adv. Space Res.*, 2015, vol. 55, no. 8, pp. 2020–2032.

Klimenko, V.V., Karpachev, A.T., Klimenko, M.V., Ratovskii, K.G., and Korenkova, N.A., Latitudinal structure of the longitudinal effect in the nighttime ionosphere during the summer and winter solstice, *Russ. J. Phys. Chem. B*, 2016, vol. 10, no. 1, pp. 91–99.

Lei, J., Thayer, J.P., and Forbes, J.M., Longitudinal and geomagnetic activity modulation of the equatorial thermosphere anomaly, *J. Geophys. Res.*, 2010, vol. 115, A08311. doi 10.1029/2009JA015177

Liu, H., Stolle, C., Forster, M., and Watanabe, S., Solar activity dependence of the electron density at 400 km at equatorial and low latitudes observed by CHAMP, *J. Geophys. Res.*, 2007, vol. 112, A11311. doi 10.1029/2007JA012616

Lockwood, G.E.K. and Nelms, G.L., Topside sounder observations of the equatorial anomaly in the 75° W longitude zone, *J. Atmos. Terr. Phys.*, 1964, vol. 26, no. 5, pp. 569–580.

Lyon, A.J. and Thomas, L., The *F*2-region equatorial anomaly in the African, American and East Asian sectors during sunspot minimum, *J. Atmos. Terr. Phys.*, 1963, vol. 25, no. 7, pp. 373–386.

Matuura, N., Characteristics of global distribution of *foF*2, *Sol. Terr. Environ. Res. Jpn.*, 1981, vol. 5, pp. 35–38.

Oh, S.-J., Kil, H., Kim, W.-T., Paxton, L.J., and Kim, Y.H., The role of the vertical E × B drift for the formation of the longitudinal plasma density structure in the low-latitude *F* region, *Ann. Geophys.*, 2008, vol. 26, no. 7, pp. 2061–2067.

Pancheva, D. and Mukhtarov, P., Global response of the ionosphere to atmospheric tides forced from below: Recent progress based on satellite measurements global tidal response of the ionosphere, *Space Sci. Rev.*, 2012, vol. 168, nos. 1–4, pp. 175–209.

Rajaram, G., Structure of the equatorial *F*-region, topside and bottomside—a review, *J. Atmos. Terr. Phys.*, 1977, vol. 39, no. 9, pp. 1125–1144.

Ram, S.T., Su, S.-Y., and Liu, C.H., FORMOSAT-3/COSMIC observations of seasonal and longitudinal variations of equatorial ionization anomaly and its interhemispheric asymmetry during the solar minimum period, *J. Geophys. Res.*, 2009, vol. 114, A06311. doi 10.1029/2008JA013880

Rao, B.C.N., Some characteristic features of the equatorial ionosphere and the location of the *F*-region equator, *J. Geophys. Res.*, 1963, vol. 68, no. 9, pp. 2541–2549.

Rao, C.S.R. and Malthotra, P.L., A study of geomagnetic anomaly during I.G.Y., *J. Atmos. Terr. Phys.*, 1964, vol. 26, no. 11, pp. 10751085.

Rastogi, R.G., Chandra, H., Sharma, R.P., and Rajaram, G., Ground-based measurements of ionospheric phenomena associated with the equatorial electrojet, *Indian J. Radio Space Phys.*, 1972, vol. 1, no. 2, pp. 119–135.

Ren, Z., Wan, W., Liu, L., and Chen, Y., and Le, H., Equinoctial asymmetry of ionospheric vertical plasma drifts and its effect on *F*-region plasma density, *J. Geophys. Res.*, 2011, vol. 116, A02308. doi 10.1029/2010JA016081

Rush, C.M., Rush, S.V., Lyons, L.R., and Venkateswaran, S.V., Equatorial anomaly during a period of declining solar activity, *Radio Sci.*, 1969, vol. 4, no. 9, pp. 829–841.

Sastri, J.H., Equatorial anomaly in *F*-region—a review, *Indian J. Radio Space Phys.*, 1990, vol. 19, no. 4, pp. 225–240.

Sharma, R.P. and Hewens, E.J., A study of the equatorial anomaly at American longitudes during sunspot minimum, *J. Atmos. Terr. Phys.*, 1976, vol. 38, no. 5, pp. 475–484.

Su, Y.Z., Oyama, K.-I., Bailey, G.J., Fukao, S., Takahashi, T., and Oya, H., Longitudinal variations of the topside ionosphere at low latitudes: Satellite measurements and mathematical modelings, *J. Geophys. Res.*, 1996, vol. 101, no. 8, pp. 17191–17205.

Tsai, L.-C., Liu, C.H., Hsiao, T.Y., and Huang, J.Y., A near real-time phenomenological model of ionospheric electron density based on GPS radio occultation data, *Radio Sci.*, 2009, vol. 44, RS5002. doi 10.1029/2009RS004154

Walker, G.O., Longitudinal structure of the *F*-region equatorial anomaly—a review, *J. Atmos. Terr. Phys.*, 1981, vol. 43, no. 8, pp. 763–774.

Walker, G.O., Ma, J.H.K., and Golton, E., The equatorial ionospheric anomaly in electron content from solar minimum to solar maximum for South East Asia, *Ann. Geophys.*, 1994, vol. 12, nos. 2–3, pp. 195–209.

Wu, Q., Killeen, T.L., and Spencer, N.W., Dynamics Explorer 2 observations of equatorial thermospheric winds and temperatures: Local time and longitudinal dependencies, *J. Geophys. Res.*, 1994, vol. 99, no. 4, pp. 6277–6288.

Yizengaw, E., Moldwin, M.B., Sahai, Y., and Rodolfo, J., Strong postmidnight equatorial ionospheric anomaly observations during magnetically quiet periods, *J. Geophys. Res.*, 2009, vol. 114, A12308. doi 10.1029/2009JA014603

Yue, X., Schreiner, W.S., Kuo, Y.-H., and Lei, J., Ionosphere equatorial ionization anomaly observed by GPS radio occultations during 2006–2014, *J. Atmos. Terr. Phys.*, 2015, vol. 129, no. 7, pp. 30–40.

Zhao, B., Wan, W., Liu, L., and Ren, Z., Characteristics of the ionospheric total electron content of the equatorial ionization anomaly in the Asian–Australian region during 1996–2004, *Ann. Geophys.*, 2009, vol. 27, no. 10, pp. 3861–3873.

Translated by O. Pismenov